Physicochemical characterization of three natural clays used as adsorbent for the humic acid removal from aqueous solution

Soumahoro Gueu, Gisele Finqueneisel, Thierry Zimny, Daniele Bartier, Benjamin Kouassi Yao

Adsorption Science & Technology

Research Article

Adsorption Science & Technology
2019, Vol. 37(1–2) 77–94

DOI: 10.1177/0263617418811469
journals.sagepub.com/home/adt
SAGE

Physicochemical characterization of three natural clays used as adsorbent for the humic acid removal from aqueous solution

Soumahoro Gueu
Laboratoire de Chimie et Physique Approche Multi-échelle des Milieux Complexes (LCPA2MC), Université de Lorraine, Institut Jean Barriol, Saint-Avold, France; Laboratoire des Procédés Industriels de Synthèse, Institut National Polytechnique Félix Houphouët-Boigny, de l'Environnement et des Energies Nouvelles (LAPISEN), Yamoussoukro, Côte d'Ivoire

Gisèle Finqueneisel and Thierry Zimny
Laboratoire de Chimie et Physique Approche Multi-échelle des Milieux Complexes (LCPA2MC), Université de Lorraine, Institut Jean Barriol, Rue Victor Demange, Saint-Avold, France

Danièle Bartier
GeoRessources, Université de Lorraine, Vandoeuvre-les-Nancy, France

Benjamin Kouassi Yao
Laboratoire des Procédés Industriels de Synthèse, Institut National Polytechnique Félix Houphouët-Boigny, Yamoussoukro, Côte d'Ivoire

Abstract

Adsorption behaviours of humic acid on three natural clays from Ivory Coast were studied. In order to investigate the adsorption mechanism, characterization of clays and the humic acid–clay

Corresponding author:
Benjamin Kouassi Yao, Institut National Polytechnique Félix Houphouët-Boigny – Laboratoire des Procédés Industriels de Synthèse, de l'Environnement et des Energies Nouvelles (LAPISEN), BP 1093 Yamoussoukro, Côte d'Ivoire.
Email: benjamin.yao@inphb.ci

complex was conducted by using various analytical methods (attenuated total reflectance Fourier transform infrared spectroscopy (ATR-FTIR), X-ray diffraction (XRD), specific surface area analysis (BET) and chemical composition). As a result, adsorption process showed that the maximum adsorption capacity of humic acid was achieved at pH = 3 and was found to be to 115 mg/g obtained for the best sample. For all clays, the adsorption was found to be strongly dependent on pH and well fitted by the Langmuir model. In addition, it was shown that the adsorption capacity was linked to the kaolinite content of each sample. The results showed that humic acid adsorption onto clay was made via electrostatic interactions, ligand exchange and hydrophobic interactions. This study showed that clays are valuable adsorbents for the removal of humic acid.

Keywords
Clay mineral, adsorption, humic acid, electrostatic interactions, ligand exchange

Submission date: 4 July 2018; Acceptance date: 8 October 2018

Introduction

Humic substances (HSs) are derived from the microbial degradation of plants and animals. They constitute the main components of natural organic matter. HSs are polyfunctional, including groups such as carboxylic and phenolic, present a high aromatic degree (Shen et al., 2016; Zhang et al., 2012). Humic acid (HA), one of the major constituents of HS, is a problem for the water supply industry. It affects water quality by undesirable coloration, odour and taste. When present in water, HA serves as a nutrient for microorganisms contributing to bacterial growth in water distribution systems. Also, it binds to pesticides and herbicides to increase the concentrations of these substances and promote their transport in water. In the presence of chlorine, HA leads to the formation of byproducts of disinfection, of which trihalomethanes are known as human carcinogens (Lin and Zhan, 2012). Thus, the minimization of HA concentration in drinking water finds all importance and interest.

Various treatment methods have been developed to remove HA from water. The most used are adsorption, coagulation–flocculation, membrane separation, biodegradation, ion exchange and photocatalysis. Adsorption is one of the popular techniques for the HA elimination due to its efficiency and its easy implementation. Many kinds of adsorbents have been used including activated carbons (Bouras et al., 2015), zeolites (Wang et al., 2008), resins (Wang et al., 2010), chitosan (Yan and Bai, 2005) and clay mineral (Abate and Masini, 2003; Elfarissi and Pefferkorn, 2000; Feng et al., 2005). Among the adsorbents mentioned above, the clay is gaining increasing interest from researchers (Chen et al., 2017; Peng et al., 2005; Salman et al., 2007; Wang et al., 2012; Zhang et al., 2012).

Various behaviours of HA adsorption have been observed. Feng et al. (2005) reported that kaolinite displayed higher adsorption for peat HA than montmorillonite under the same experimental conditions. They explained these results by selective adsorption and different binding mechanisms of HA. Zhang et al. (2012) studied the fulvic and HA adsorption on kaolinite, smectite and vermiculite. The authors demonstrated that smectite had greater adsorption capacity followed by vermiculite and kaolinite and make a link between adsorption ability and clay structure. Kaolinite presented the smallest specific surface (1.96 m^2/g) and a relatively flat and smooth surface, therefore owning the weakest

adsorption ability. Smectite displayed the largest specific surface (19.09 m^2/g) and thus had strong adsorption ability towards HA. However, even if many studies about HA adsorption onto various clay minerals exist, the question about the best adsorbent for humic substance between kaolinite and smectite is not elucidated. Therefore, it is important to continue studying the adsorption mechanism of humic substances on clay minerals. Organic material can be adsorbed to clay surfaces through six mechanisms: ligand exchange, cation bridges (including water bridges), anion exchange, cation exchange, van der Waals interactions and hydrogen bonding (Zhou et al., 1994). Although many studies investigated the adsorption behaviours of organic material–clay mineral, relatively few of them studied the mechanism in detail. A better characterization of both clays and HA–clay complexes is imperative to enhance understanding of adsorption processes and then examine the adsorption mechanism of HA on clays.

The adsorption of HA is largely carried out with commercial clays (Abate and Masini, 2003; Chen et al., 2017; Feng et al., 2005; Wang et al., 2012; Zhang et al., 2012). By using natural clays for the elimination of HA, this work fills a vacuum in the literature.

The main target of this study was to identify the efficient natural clay adsorbent towards HA. This work also examines how clay structure impacts the adsorption capacity. In addition, HA–clay complex was analysed in order to propose a mechanism regarding their interactions. Also, the effect of initial concentration of HA, effect of contact time, pH and temperature on HA adsorption was discussed.

Materials and methods

Materials

Water and chemicals. Distilled water (electrical conductivity = 0.35 μS/cm) was used throughout the experimental studies. HA was purchased from Sigma-Aldrich in solid form. H_2O_2 50% was provided by Solvay; HCl (37% purity) and NaOH (>99% purity) were sourced from Merck. $AgNO_3$ (99.8% purity) and cobalt hexamminecobalt (III) chloride were supplied by Panreac and NaCl (99.5% purity) was obtained from Euclid Chemical. All reagents used were of analytical grade.

HA solution. One hundred and fifty grams of HA were dissolved into 1 L of distilled water (usually after stirring during 14 hours), then it was filtered through a 0.45 μm nylon filter to remove eventually undissolved HA particles. The HA solution obtained was kept away from light for future experiments.

Raw clays. The three clays used in this study came from Ivory Coast on natural deposits. The first clay was a kaolin whitish-coloured designated Y. The second, designated D, was gray colour. The last sample was orange–red coloured and was designated K. These designations (Y, D and K) are in fact the first letters of the names of the cities (Yamoussoukro, Dabou and Katiola) from which these clays came. The original material was stirred in distilled water until obtaining clay dispersion, then poured to pass through 50 μm sieve and dried at 105°C. The obtained clays were called 'raw clays' and underwent purification treatments in order to obtain size particles less than 2 μm rich in clay minerals.

Clay purification. The raw clays (<50 μm fraction) were first treated by 50% hydrogen peroxide in order to reduce organic matter and treated by 0.5 N hydrochloric acid to destroy carbonates. In addition, the samples were made homoionic by suspension in a 1 mol/L NaCl during 24 hours to ensure a complete exchange of sodium ions. The excess salt was removed by washing repeatedly clay slurry with distilled water and centrifuging at 5300 r/min for 5 minutes until the supernatant became cloudy and free from chlorides (confirmed by $AgNO_3$ test).

The fine fraction of clay (particle size <2 μm) was extracted by placing a suspension of exchanged clay in a glass tube to allow the particles to sediment according to Stokes' law (Holtzapffel, 1985) represented as:

$$t = 190 \ \frac{x}{d^2} \tag{1}$$

where t: time (min), x: depth (cm), d: particle size (μm).

After 950 minutes, the supernatant at a depth of 20 cm was removed up. The <2 μm fine-clay mineral fraction was recovered by drying the supernatant in an oven at 105°C during 24 hours. The obtained sodium saturated clays were designated as Y-Na^+, D-Na^+ and K-Na^+.

Methods of analysis

X-ray diffraction (XRD) patterns of all samples were recorded at room temperature, using a Cu Kα radiation D2 Phaser Bruker diffractometer equipped with LYNXEYE detector, under 30 kV and 10 mA. The analyses were performed on bulk-rock powdered samples over the 2θ angular range [2.5–70] using a scan step of 0.02° 2θ with an exposure time of 0.6 seconds and on clay fraction (<2 μm) between [2.5–30°] 2θ with a scan step of 0.01° 2θ and an exposure time of 0.6 seconds. The identification of clay minerals was made according to the modification of the (001) series of basal reflections position on X-ray diffractograms (air drying, ethylene glycol saturation and heating to 490°C for 2 hours). The relative content of clay minerals in the fine fraction (<2 μm) was conducted using a semi-quantitative analysis according to the method described by Holtzapffel (1985). The error made on these percentage is about 5–10%.

Attenuated total reflectance Fourier transform infrared spectroscopy (ATR_FTIR) was performed from 4000 to 400 cm^{-1} using 64 scans and a resolution of 4 cm^{-1} with a Bruker Alpha spectrometer.

The chemical compositions of raw clays and purified fraction were determined by means of an Inductively Coupled Plasma–Optical Emission Spectrometer (ICP–OES) Varian model 725. The specific surface area of samples was determined from nitrogen adsorption/desorption isotherms at −196°C, obtained from a Quantachrome type Autosorb IQ device, after outgassing the samples at 150°C for 12 hours under vacuum. The cation exchange capacity (CEC) of the clays was determined according to the method based on cobalt hexammonium chloride adsorption described by Ciesielski et al. (1997).

Adsorption experiments

The adsorption studies of HA onto clays were conducted by batch technique in the presence of 1 g/L of clays at pH = 3 and T = 25°C. Kinetic studies were carried out with initial HA

solution concentrations in the range of 10–100 mg/L. After predefined contact time, a definite volume (3 mL) of the solution was withdrawn and centrifuged during 15 minutes at 5300 r/min. The residual concentration of HA in the supernatant was measured by a UV/Vis spectrophotometer (UV–visible Biochrom Libra S12) at 254 nm.

In order to investigate the concentration of HA during experiment, the following calibration curve was: $y = 0.0267\ x - 0.0016$ ($R^2 = 0.9999$), where: y is the absorbance at 254 nm, x is the HA concentration (mg/L) and R^2 is the correlation coefficient.

The amounts of HA adsorbed at time t, q_t (mg/g) were calculated using the following equation:

$$q_t = \frac{(C_0 - C_t).\ V}{m} \tag{2}$$

where C_0 is the initial concentration of HA solution (mg/L), C_t is the HA concentration at any time t (mg/L), V is the solution volume (L) and m is the adsorbent weight (g).

These experiments were done in order to find the equilibrium time between the adsorbent and the HA solution. The adsorption equilibrium is considered to be achieved when the difference between the amounts of HA adsorbed for two consecutive times does not exceed 0.5 mg/g. Each adsorption test was repeated three times under the same experimental conditions and the result corresponds to the average.

The pH of the solution is a very important factor because it affects the surface charge of the adsorbents as well as the ionization of the different pollutants. Change in pH affects the adsorptive process through dissociation of functional groups of the active sites on the surface of the adsorbent (Wang et al., 2012). In order to determine the favourable pH value, in terms of maximum adsorption capacity, the pH of HA solution was investigated between 3 and 10 following the next process: 300 mg of clay was added to 300 mL of HA solution (50 mg/L) at fixed temperature (20°C). The initial pH value of HA was adjusted by adding NaOH (0.1 M) or HCl (0.1 M). The adsorbed amounts of HA were then determined after 6 hours of equilibrium time using equation (1).

Adsorption isotherms were investigated at pH equal to 3 in presence of 300 mg of clay and 300 mL of HA solutions by increasing initial concentrations (10–230 mg/L). After 6 hours of agitation, the solutions were centrifuged during 15 minutes at 5300 r/min and the supernatant was taken to determine the adsorbed amount as described above.

The effect of temperature on the adsorption behaviour was explored at 20°C, 27°C and 35°C and for 50 mg/L HA concentration. The procedure was identical to that mentioned above but in this case, the flask was left stirring during 6 hours till equilibrium was established.

Results and discussion

Material characterization

The XRD diffractogram of all raw samples (Figure 1) showed reflections assigned to kaolinite, quartz and illite. They contained accessory minerals like feldspar for samples Y and D, and like goethite for the sample K.

Diffractograms of the <2 μm fraction are presented in Figure 2(a), (b) and (c). The sample Y-Na^+ is constituted of kaolinite and illite, while D-Na^+ contained kaolinite,

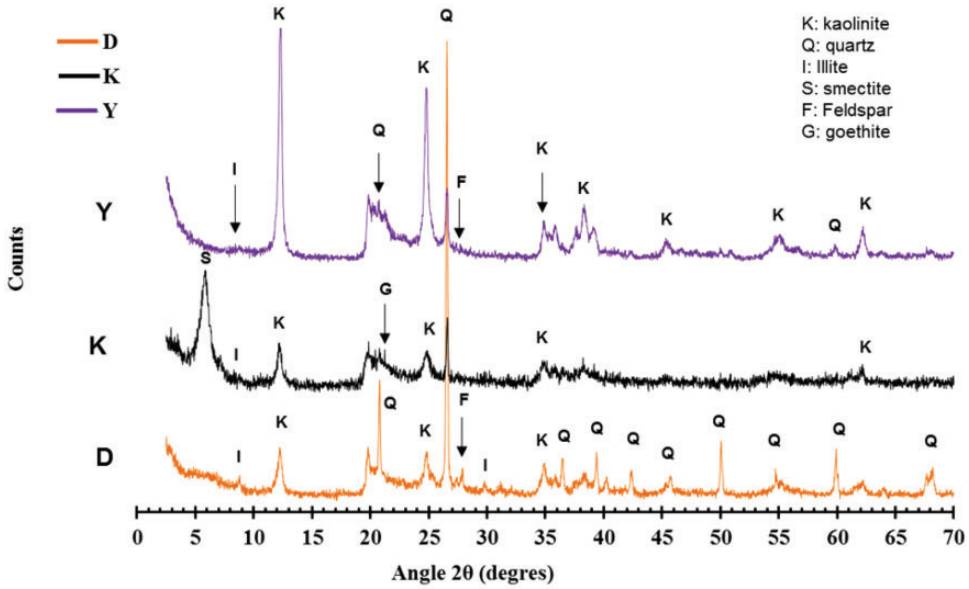

Figure 1. XRD diffractograms of raw clays.

illite and smectite. Like the previous samples, K-Na^+ displayed kaolinite, illite and smectite. In addition, it presented also a regular illite/smectite mixed layer minerals. It should be noted that on diffraction patterns of <2 μm fractions, there were no reflections corresponding to detrital tectosilicates initially present in the raw clays. This observation indicated that the purification method employed here was appropriate.

Semi-quantitative analysis of the clay fraction is reported in Table 1. Samples Y-Na^+ and D-Na^+ are mostly constituted of kaolinite (95% and 70% respectively). Those results are consistent with those obtained by Andji et al. (2009) (48–81% of kaolinite) and by Coulibaly et al. (2008) (56–82% of kaolinite). Sample Y-Na^+ shows greater kaolinite purity comparable to a commercial kaolinite KGa-2 (95–100% of kaolinite) as reported by Chen et al. (2017). Sample K-Na^+ contains a significant amount of smectite (50%). This value is much lower than those mentioned by Kpangni et al. (2008) concerning two raw clays K1 and K2 (74 and 73.4% of montmorillonite, respectively).

Other characteristics measured on clays studied are listed in Table 2. Chemical compositions (SiO_2 30%, Al_2O_3 52%, Fe_2O_3 4%) of sample D are of the same order of magnitude than those obtained by Coulibaly et al. (2008) (SiO_2 27.7%, Al_2O_3 56.2%, Fe_2O_3 6.6%). Sample Y composition is similar to that of D; nevertheless Y is slightly rich in alumina (34.90%) and poor in iron (1.93%). For K sample, the percentages of silica and iron oxides are consistent with those provided for clays K1 (SiO_2 48.35%, Fe_2O_3 13.43%) and K2 (SiO_2 47.98%, Fe_2O_3 13.81%) (Kpangni et al., 2008). However, Al_2O_3 content is lower in samples K1 (14.36%) and K2 (17.58%) than those obtained in this study.

The SiO_2/Al_2O_3 ratios, ranging from 1.34 to 2.00, are lower than those of Bikougou (2.21, Eba et al., 2011), or for bentonite (2.74, Vojkan et al., 2017) or also for K1 and K2 (3.37 and 2.73 respectively, Kpangni et al., 2008).

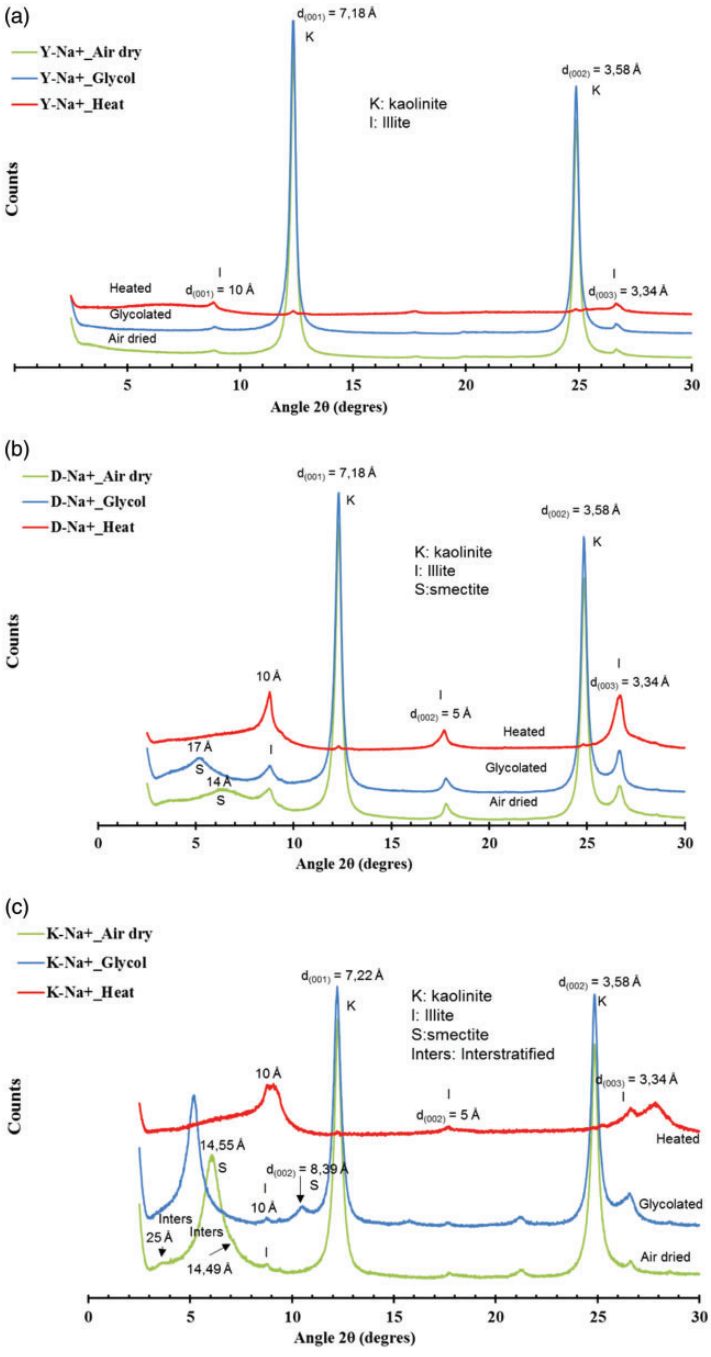

Figure 2. XRD patterns of purified samples: (a) Y-Na^+; (b) D-Na^+ and (c) K-Na^+.

Table 1. Mineralogical composition of clay samples (%).

	Kaolinite	Illite	Quartz	Feldspar	Smectite	Illite–smectite	Goethite
Y	68	8	16	8	0	0	0
Y-Na^+	95	5	0	0	0	0	0
D	16	15	57	8	4	0	0
D-Na^+	70	15	0	0	15	0	0
K	12	3	8	0	63	12	2
K-Na^+	40	5	0	0	50	5	0

Table 2. Chemical composition, Brunauer–Emmett–Teller (BET) specific surface area (S_{BET}) and cation exchange capacity (CEC) of studied clays.

% by weight	Y	Y-Na^+	D	D-Na^+	K	K-Na^+
SiO_2	48.90	43.70	52.00	45.30	45.00	41.10
Al_2O_3	34.90	32.50	30.80	29.50	22.50	20.50
Fe_2O_3	1.93	2.01	4.44	6.12	13.90	13.50
K_2O	0.70	0.68	1.47	1.65	0.62	0.59
CaO	0.05	1.34	0.20	0.86	0.42	1.62
Na_2O	0.11	0.63	0.46	1.16	0.04	1.94
TiO_2	0.91	1.00	1.12	0.71	0.98	0.72
P_2O_5	0.02	0.04	0.04	0.06	0.01	0.05
MgO	0.15	0.48	0.63	0.79	1.44	1.08
Loss on ignition (%)	12.33	17.18	8.82	13.85	15.09	18.90
Si/Al	1.40	1.34	1.69	1.53	2.00	2.00
S_{BET} (m^2/g)	28.33	36.29	28.72	35.08	46.40	57.46
CEC (meq/100 g)	3.41	13.85	14.10	16.66	37.55	51.56

The low contents in K_2O, CaO, Na_2O, TiO_2, P_2O_5 and MgO are conspicuous and point to mature sediments (Boulingui et al., 2015).

In comparison with other results, it appears that the CEC value of sample Y (3.41 meq/100 g) is similar to that of Kaolinite KGa-2 (3.3 meq/100 g, Chen et al., 2017). Sample D shows a slightly higher CEC (14.10 meq/100 g), probably due to illite whose CEC is higher, 10–40 meq/100 g. For sample K, the measured CEC value (37.55 meq/100 g) is higher than that of kaolinites and illites but lower than that of smectite, 80–120 meq/100 g (Eslinger and Peaver, 1988). This is because K was a mixture of clay minerals.

The CEC values of the purified clays were higher than those of raw samples. This would be due to the sodium saturation step. It is possible that during this step, the cations Na^+ will have fixed to the surface of the clay, thus increasing the number of exchangeable cations. Similar results were presented by Jozja (2003) who found that the CEC of the raw clays of Maminas, Currila and Prrenjas, which were initially equal to 19.6, 14.6 and 65 meq/100 g had increased markedly to 46.1, 39 and 92 meq/100 g, respectively after the samples have been purified and saturated with sodium.

Specific surface area values for clays studied are lower than those of Bikougou (170 m^2/g, Eba et al., 2011) and higher than those of Mengono (10.9–21.2 m^2/g, (Boulingui et al., 2015),

or than commercials clays, Kaolinite (1.96 m^2/g), Smectite (19.09 m^2/g) (Zhang et al., 2012); Kaolinite KGa-2 (19.3 m^2/g), Montmorillonite (23.3 m^2/g) (Chen et al., 2017).

It appears by comparing each raw clay with its purified fraction that the specific surface area increases slightly due to the removal of the impurities.

Moreover, according to the classification of the International Union of Pure and Applied Chemistry (IUPAC) (Sing, 1985), the N_2 adsorption isotherms (Supplemental material, Figure 1) of all studied clays were of type II. The Brunauer–Emmett–Teller (BET) isotherms of clays showed the existence of an H3 loop hysteresis (IUPAC classification). Such isotherms are given by either slit-shaped pores or, as in the present case, assemblages of platy particles (Rouquerol et al., 1999). In addition, the pore volumes measured are very low (<0.08 cm^3/g) indicating that these materials are non-porous.

Adsorption kinetics

Kinetic studies were done by varying initial concentration of HA in the range of 10–100 mg/L with 1 g/L of clays at $pH = 3$ and 293 K. The data obtained with Y-Na^+, D-Na^+ and K-Na^+ adsorbent are represented in Figure 3(a), (b) and (c), respectively. Equilibrium time was strongly related to the initial concentration of HA. As illustrated by these curves, the equilibrium time increased with the initial concentration of adsorbate. Equilibrium time was short for initial concentrations inferior to 50 mg/L, and was estimated to 120 minutes. When initial concentrations were high ($C_0 \geq 50$ mg/L), the kinetics became slow and the time required to attain equilibrium was high, approximately 300 minutes. HA is a mixture of macromolecular organic compounds of different sizes. At low concentration, the HA molecules rapidly reached the clay surface to occupy adsorption sites. However, for greater initial concentration, adsorbates have to travel deeper looking for free sites. Chen et al. (2017) reported that the lateral repulsion becomes stronger with increasing HA adsorption and is therefore most relevant at high adsorption values due to the increasing lateral repulsion between adsorbed HA molecules. As a result, equilibrium time was higher. Moreover, an intermediate equilibrium was visible on the kinetic curves. This kinetic form, which we called 'kinetic of double plateau' has already been observed by other authors (Rauthula and Srivastava, 2011; Tang et al., 2012) but remained so far unexplained. Various studies (Feng et al., 2005; Zhang et al., 2012) have reported a selective adsorption of HA on clay minerals. Hence, intermediate equilibrium might correspond to the adsorption of HA aliphatic fractions, while the second plateau might be related to the adsorption of higher molecular weight of HA.

Adsorption of HA

pH effects. The influence of pH on HA adsorption by different purified clays was investigated to obtain further information about the adsorption process (Figure 4). It was observed for each clay that adsorption capacity had the highest value at $pH = 3$, after which the adsorption decreased continuously. For example, in the case of sample Y-Na^+, as the pH of the solution was increased from 3 to 10, the adsorbed amount of HA decreased from 39 to 8 mg/g.

One of the most important characteristics of the adsorbent is its point of zero charge (PZC) as it governs the adsorption process. The pH of PZC (pH_{PZC}) of the three studied clays was found to be 6.5, 7.0 and 6.7 for Y-Na^+, D-Na^+ and K-Na^+ respectively as

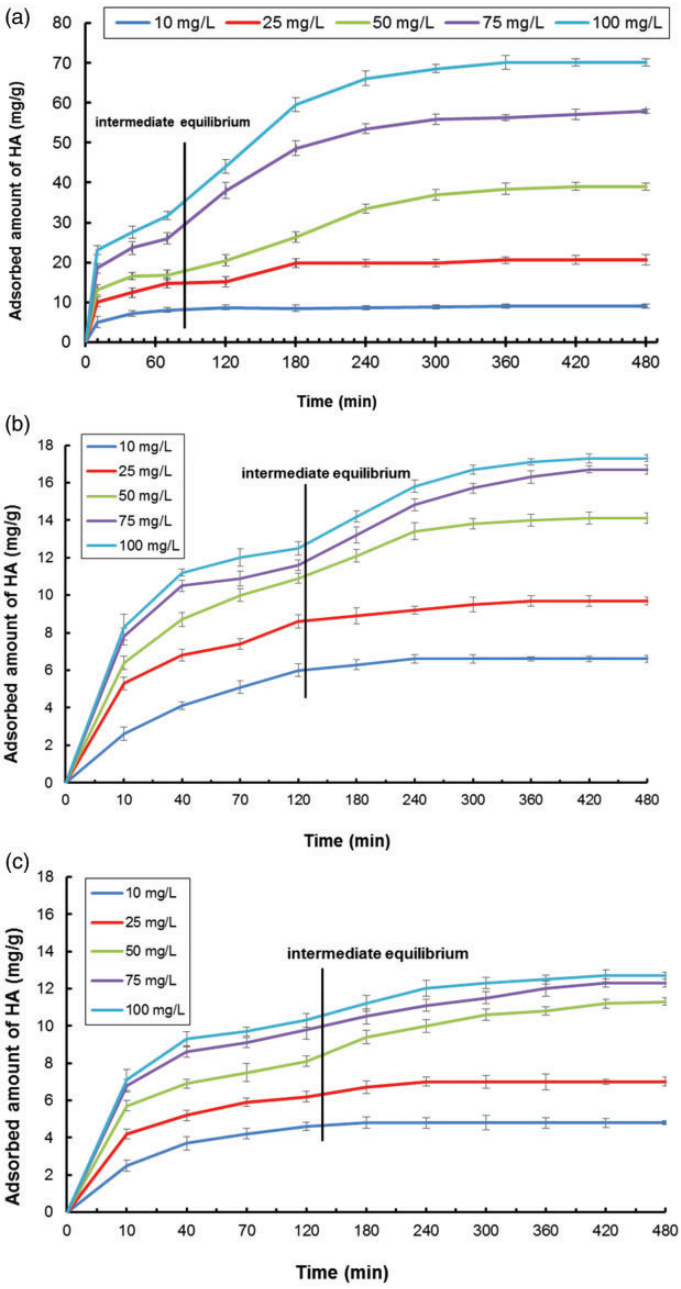

Figure 3. Effect of contact time on HA adsorption onto purified samples: (a) Y-Na^+; (b) D-Na^+ and (c) K-Na^+; vertical line indicating intermediate equilibrium. $[HA]_0 = 10–100$ mg/L, $T = 20°C$; [clay] = 1g/L, pH = 3.

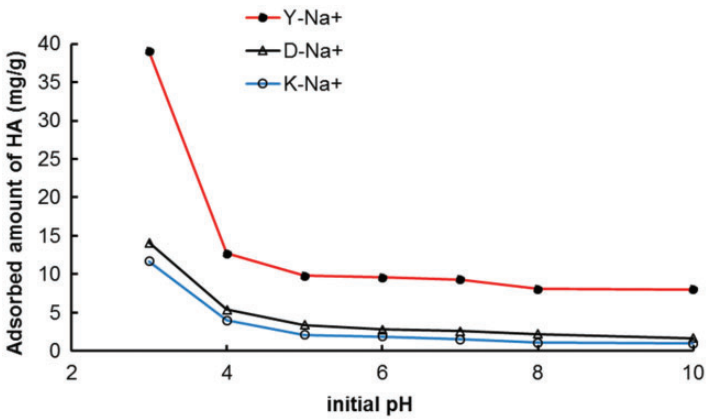

Figure 4. Effect of pH on HA adsorption. $T = 20°C$; [clay] = 1 g/L, $[HA]_0 = 50$ mg/L.

determined by the method described by Vieira et al. (2009). Therefore, the surface of these clays is positively charged below pH = 7 and negatively charged above this pH.

HA is considered to be a mixture of compounds with functional groups of weak acids, such as carboxylic and phenolic groups. Since the pKa of carboxylic and phenolic groups are about 3 and 9, respectively (Lin and Zhan, 2012), HA is then negatively charged by deprotonation of the carboxyl groups at pH above 3.

As reported in the literature (Majzik and Tombácz, 2007; Zhu et al., 2016), AlOH and SiOH are present on the surface of the clay. These sites react with H^+ and OH^- ions in the solution, and the positive Al-OH_2^+ ($Al\text{-}OH + H^+ = Al\text{-}OH_2^+$) or negative Al-$O^-$ or Si-O^- ($Al\text{-}OH + OH^- = Al\text{-}O^- + H_2O$) are generated on the surface via protolytic reactions, which is mainly dependent on the pH value of the solution (Abate and Masini, 2003).

The surface of the three clays holds positive charge at relatively lower pH values ($pH < pH_{ZPC}$) leading to the adsorption of HA molecules negatively charged. In addition, there was adsorption via ligand exchange between the HA molecule and the oxide minerals as reported in the literature (Abate and Masini, 2003; Feng et al., 2005; Zhang et al., 2012). Based on these facts, the reactions between HA and the clays could be represented as follows

$$M - OH + H^+ = M - OH_2^+$$
$$M - OH_2^+ + {}^-O - COHA = M - OH_2^+ - {}^-O - COHA$$
$$M - OH_2^+ + {}^-O - COHA = M - O - COHA + H_2O$$

where M represents Al or Si.

When increasing the solution pH value, the hydroxyl groups of the clays become less and less protonated and their surface charge reverses from positive to negative. From pH 7, the conditions of electrostatic attraction become unfavorable. However, the adsorption capacities obtained were not zero: 8; 1.7 and 1 mg/g for Y-Na^+; D-Na^+ and K-Na^+ respectively at pH 10. Therefore, adsorption of HA is difficult to be explained by electrostatic interaction since both clay and HA possess negative charge, and other mechanisms may be responsible for HA adsorption. At high pH, some hydrophobic interaction may still occur although HA has both hydrophobic and hydrophilic parts and its hydrophobic property is strong at low

pH when the acidic groups are more protonated (Schwarzenbach et al., 2005; Terashima et al., 2004). On the other hand, basal planes T of clays are basically hydrophobic (Chen et al., 2017). Hence, the adsorption of HA on clays may be attributed to hydrophobic interaction because both clays and HA possess hydrophobic parts.

To resume, in acidic medium HA adsorption mechanism may include electrostatic interaction, ligand exchange and hydrophobic interaction, while above pHzpc of clay (around 7) only hydrophobic interaction may still occur.

Adsorption isotherms. The adsorption isotherms of HA on clays surface at pH = 3 are presented in Figure 5. The three isotherms reached a saturation plateau (Figure 5) indicating an L-type isotherm according to Giles classification (Giles et al., 1974). Generally, isotherms of type L were the result of a monolayer adsorption on clays surface suggesting both isoenergetic adsorption sites and absence of lateral interactions between adsorbed molecules (Hamoud et al., 2017).

Then the common Langmuir model (equation (3)) is applied to evaluate the adsorption data (Table 3).

$$\frac{C_e}{q_e} = \frac{1}{q_m b} + \frac{C_e}{q_m} \tag{3}$$

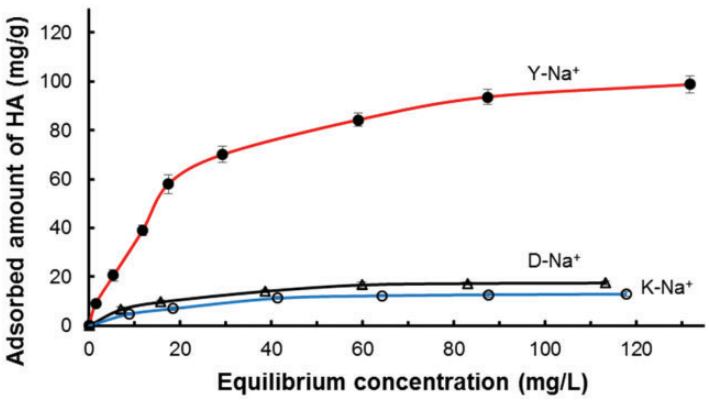

Figure 5. HA adsorption isotherms. $[HA]_0 = 10–230$ mg/L, T = 20°C; [clay] = 1g/L and pH = 3.

Table 3. Langmuir parameters for humic acid (HA) adsorption on purified clays: $[HA]_0 = 10–230$ mg/L, [clay] = 1 g/L, T = 20°C at pH = 3.

	q^a_{exp} (mg/g)	q^b_m (mg/g)	b^c (L/mg)	$R^{2,d}$	Θ^e
Y-Na^+	99 ± 3.2	115 ± 1.37	0.049 ± 0.02	0.9968	0.86
D-Na^+	17 ± 1.0	20 ± 0.01	0.066 ± 0.01	0.9976	0.85
K-Na^+	13 ± 0.7	15 ± 0.01	0.054 ± 0.01	0.9954	0.87

[a] q_{exp}: experimental adsorbed amount.
[b] q_m: adsorption capacity corresponding to monolayer coverage.
[c] b: Langmuir constant.
[d] R^2: coefficient of correlation.
[e] Θ: Langmuir coverage fraction = q_{exp}/q_m.

where q_e is the adsorbed amount of HA on clay (mg/g), C_e is the HA concentration at the equilibrium (mg/L), q_m is the maximum adsorption capacity (mg/g) and b is the Langmuir constant (L/mg).

The application of the Langmuir isotherm was suitable as the correlation coefficients R^2 were higher than 0.995. Furthermore, the q_m values of HA calculated from Langmuir model were comparable to their experimental adsorbed amounts. According to θ values, partial monolayer coverage ($\theta \approx 0.85$) on the clay surface was observed. Meanwhile, lower interactions ($b \leq 66$ L/g) and equivalent values for the three clays were found for HA adsorption.

The difference in clay's behaviour toward HA can be explained by a structural difference. The sample Y-Na^+ was mainly composed of kaolinite, a clay type 1:1 while the others contained a significant proportion of illite and smectite clays type 2:1. This result also means that HA adsorption does not imply interlayer space but certainly the accessible faces and edges. Both clay types display functional groups (Al-OH, Si-OH) on their edge. From smectite configuration (TOT), only T face is accessible since O face is located between two T faces. However, minor isomorphic substitution in the tetrahedral sheet results in a few permanent negative charges on the T face. This makes T face not suitable for HA adsorption. Face O of kaolinite shows surface hydroxyl (Chen et al., 2017), which is potential adsorption site since the functional group (Al-OH) is known to have pH-dependent charge (Tombácz and Szekeres, 2006). This difference of configuration leads clays type 1:1 to have many adsorption sites compared to clay type 2:1.

Similar results were obtained by different authors (Feng et al., 2005; Zhou et al., 1994) who found that under same study conditions, kaolinite had displayed a higher adsorption capacity of humic substances than montmorillonite. Then, kaolinite content should play an important role in adsorption phenomena. However, these observations are different from some results described in the literature (Chen et al., 2017; Zhang et al., 2012). Chen et al. (2017) have found that at pH = 4, similar maximum adsorptions (361 and 342 mg/g respectively) were observed for kaolinite and montmorillonite; but at pH = 6 and 8, the maximum adsorption on montmorillonite (323 and 281 mg/g, respectively) was significantly higher than that on kaolinite (209 and 171 mg/g, respectively).

Moreover, if the difference in kaolinite content between Y-Na^+ and K-Na^+ is great, it was not the case between Y-Na^+ and D-Na^+. But Y-Na^+ had greater capacity than other one. To explain this difference, kaolinite crystallinity index which is a good parameter to express kaolinite order was investigated. The structural order–disorder of kaolinite was determined by FWHM (001) method developed by Amigo et al. (1994) and were 0.27, 0.36 and 0.41 for Y-Na^+, D-Na^+ and K-Na^+, respectively. These results showed that sample Y-Na^+ had better crystallinity, and that means this sample was well-ordered kaolinite. This reason could additionally explain the difference in adsorption behaviour between Y-Na^+ and D-Na^+.

The adsorption capacities of the samples D-Na^+ and K-Na^+ were lower than those found by other studies (45 mg/g, (Ghabbour et al., 1998); 70 mg/g, (Salman et al., 2007) or 68.2 mg/g, (Wang et al., 2008)) while that obtained with Y-Na^+ was higher. However, the adsorption capacities obtained in this study are very lower compared to those found by other authors mentioned in the literature (537 mg/g, (Peng et al., 2005) or 361 mg/g, (Chen et al., 2017)). It should be noted that the initial concentrations of HA used by these authors were extremely high, 1300 and 1406 mg/L, respectively.

Thermodynamic parameters. The equilibrium adsorption of HA on clays was investigated at three different temperatures (20°C, 27°C and 35°C) with an HA initial concentration of 50 mg/L and clay dosage 1 g/L.

The values of thermodynamic parameters such as change in Gibbs free energy (ΔG°), enthalpy (ΔH°) and entropy (ΔS°) were calculated using the following equations ((4) and (5)) to estimate what process will occur spontaneously.

$$\mathrm{Ln}k_d = -\frac{\Delta H^\circ}{RT} + \frac{\Delta S^\circ}{R} \tag{4}$$

$$\Delta G^\circ = \Delta H^\circ - T\Delta S^\circ \tag{5}$$

where k_d is the distribution coefficient (mL/g) and equal to q_e/C_e, R is the universal gas constant (8.314 J/mol K), and T is the reaction temperature (K).

The values of ΔH° and ΔS° are obtained from the slope and intercept of the line plotted by $\ln(k_d)$ versus 1/T, respectively. The obtained thermodynamic parameters obtained are listed in Table 4.

The positive values of ΔS° suggested that the organization of the adsorbate at the solid/solution interface became more random during the adsorption process in the temperature range studied (Lin and Zhan, 2012). The positive value of the enthalpy showed that the adsorption process was endothermic in nature. The low enthalpy values (<13.2 kJ/mol) for D-Na^+ and K-Na^+ clays indicated that the interactions might be physical adsorption due to electrostatic attraction and hydrogen bonding. Concerning Y-Na^+ sample, the enthalpy value was higher (35 kJ/mol) and due in this case to the sum of various bond energies including electrostatic attraction, ligand complexation, etc. Hydrophobic interactions may be another mechanism, as suggested above. This becomes very plausible, especially since the thermodynamic data have shown an entropy-driven process which is a characteristic of this kind of mechanism (Chen et al., 2017). The negative values of ΔG° at all temperatures indicated the feasibility of the adsorption of HA on adsorbents and the spontaneous nature of the adsorption process (Lin and Zhan, 2012).

FTIR analyses

In order to obtain more details on interactions nature between HA and clays, infrared spectroscopy analyses (in ATR mode) were done. IR spectra of Y-Na^+ before and after the adsorption and HA are shown in Figure 6.

Table 4. Thermodynamic parameters.

	ΔH° (kJ/mol)	ΔS° (J/mol.K)	ΔG° (kJ/mol)		
			20°C	27°C	35°C
Y-Na^+	35.3	188.2	−19.8	−21.1	−22.6
D-Na^+	13.2	94.1	−14.4	−15.0	−15.8
K-Na^+	10.9	83.9	−13.6	−14.2	−14.9

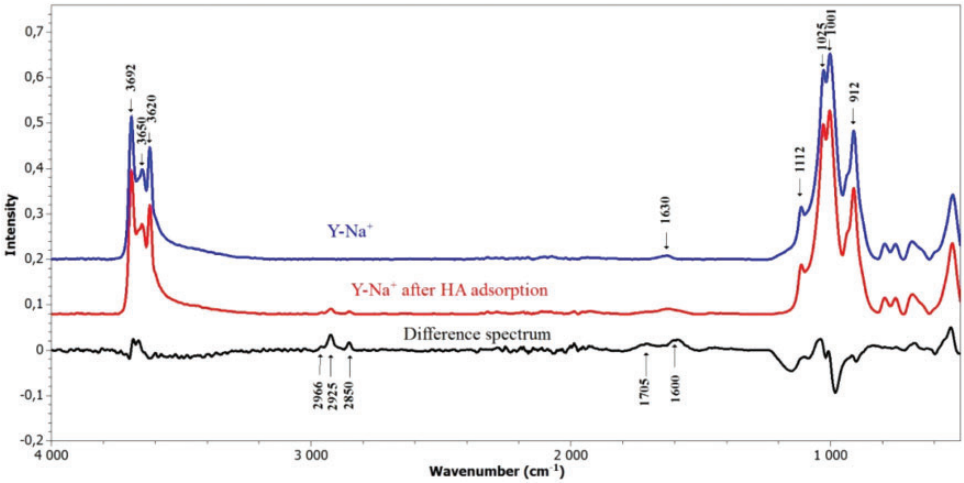

Figure 6. FT-IR spectra of bare Y-Na^+ and Y-Na^+ after HA adsorption. The difference spectrum corresponded to Y-Na^+ after HA adsorption – Y-Na^+. Conditions: pH = 3; $[HA]_0$ = 250 mg/L.

The absorption bands of clay, the characteristic frequencies and their chemical identification were attributed by referring to Madejova and Komadel (2001). The FTIR spectrum of bare Y-Na^+, taken as reference showed OH stretching of inner surface hydroxyl groups (3692 and 3650 cm^{-1}), OH stretching of inner hydroxyl groups (3620 cm^{-1}) and OH deformation of inner hydroxyl groups (912 cm^{-1}), known to be characteristic peaks of kaolinite. Bands centred at 1112 and 1001 cm^{-1} were referred to Si–O stretching vibrations and Si–O–Si or Si–O–Al lattice vibrations, respectively. Further, bands in low range of frequency (<800 cm^{-1}) can be attributed to different Si–O and Al–O vibrations. The band around 1630 cm^{-1} was assigned to physically adsorbed water and then to the H–O–H bending vibration.

For HA FTIR spectrum (Supplemental material, Figure 2), absorbance bands are observed at 3420 cm^{-1} (O–H stretching of carboxyl, phenol and alcohol), 2925 and 2850 cm^{-1} (aliphatic C–H stretching), 1556 and 1369 cm^{-1} (COO^- carbonate stretching modes) (Shen et al., 2016).

After adsorption of HA solution at pH = 3, most of carbonates species are removed and broad absorption band appeared at 1730–1600 cm^{-1}, which can be attributed to ester formation between carbonates and hydroxyl groups (see difference spectrum on Figure 6).

It is also interesting to note that after HA adsorption, three additional vibrations bands appeared at 2966, 2925 and 2850 cm^{-1}. These bands corresponded to aliphatic C–H stretching vibration of HA (Shen et al., 2016). The appearance of these three bands confirmed the fixation of HA by clay sample. This result indicated that HA was successfully adsorbed onto the clay.

These findings appear in line with the results from Zhang et al. (2012) and from Zhu et al. (2016) who concluded that ligand exchange might be an important mechanism for HA adsorption on kaolinite. The Si(Al)–O vibration modes were not affected when HA is bonded to the clay surface. Moreover, the peaks at wavenumbers 3470 and 1637 cm^{-1} (H–O–H vibrations) were not modified after adsorption. This suggests that the adsorption of HA molecules might not be controlled by hydrogen bonding.

Conclusion

In this study, three natural clays were used as adsorbent to remove HA pollution from potable water. After purification and a complete characterization, the obtained clays exhibit very different mineralogical composition in kaolinite, illite and smectite.

The main results of this study will enhance our comprehension of the interactions between HA and clay minerals. The HA adsorption was depended on different experimental parameters (pH, temperature, initial concentrations...). We showed that HA adsorption was favourable at pH 3 and occurred via electrostatic attractions, ligand exchange and hydrophobic interactions. On the kinetic curves, a 'double plateau' was shown at higher initial concentrations indicating that two different mechanisms seem to take place. According to the literature, we suggest that the aliphatic fraction of HA will be absorbed in first following by the adsorption of higher molecular weight molecules corresponding to the second plateau.

Finally, we can conclude that the purified clay with higher kaolinite percentage (95%) exhibited higher capacity due to their structure and could be an excellent adsorbent for HA removal from water.

Acknowledgements

The authors wish to thanks the Embassy of France in Ivory Coast (SCAC) and Ivorian government for the PhD research grant of Soumahoro GUEU. They sincerely thank Professor Patrick Drogui (INRS-ETE, Canada) for his great contribution to the characterization of the samples.

Declaration of Conflicting Interests

The author(s) declared no potential conflicts of interest with respect to research, authorship, and/or publication of this article.

Funding

The author(s) received no financial support for the research, authorship, and/or publication of this article.

Supplemental Material

Supplemental material is available for this article online.

References

Abate G and Masini JC (2003) Influence of pH and ionic strength on removal processes of a sedimentary humic acid in a suspension of vermiculite. *Colloids and Surfaces A: Physicochemical and Engineering Aspects* 226(1): 25–34.

Amigo JM, Bastida J, Sanz A, et al. (1994) Crystallinity of lower cretaceous kaolinites of Teruel (Spain). *Applied Clay Science* 9(1): 51–69.

Andji JYY, Toure AA, Kra G, et al. (2009) Variability of clays from Gonioubé deposit (Ivory Coast). *Journal of Applied Sciences* 9(7): 1238–1247.

Boulingui JE, Nkoumbou C, Njoya D, et al. (2015) Characterization of clays from Mezafe and Mengono (Ne-Libreville, Gabon) for potential uses in fired products. *Applied Clay Science* 115: 132–144.

Bouras HD, Benturki O, Bouras N, et al. (2015) The use of an agricultural waste material from Ziziphus jujuba as a novel adsorbent for humic acid removal from aqueous solutions. *Journal of Molecular Liquids* 211: 1039–1046.

Chen H, Koopal LK, Xiong J, et al. (2017) Mechanisms of soil humic acid adsorption onto montmorillonite and kaolinite. *Journal of Colloid and Interface Science* 504: 457–467.

Ciesielski H, Sterckeman T, Santerne M, et al. (1997) Determination of cation exchange capacity and exchangeable cations in soils by means of cobalt hexamine trichloride. Effects of experimental conditions. *Agronomie-Sciences Des Productions Vegetales et de L'Environnement* 17(1): 1–8.

Coulibaly Y, Dauscher A, Lenoir B, et al. (2008) Characterization of the clays from Abidjan region: Comparative study of some gites and their prospects for valorisation. *Revue Ivoire Science Technologie* 11: 177–192.

Eba F, Aubin Ondo J, Gueu S, et al. (2011) Treatment of aqueous solution of lead content by using natural mixture of kaolinite-albite-montmorillonite-illite clay. *Journal of Applied Sciences* 11: 2536–2545.

Elfarissi F and Pefferkorn E (2000) Kaolinite/humic acid interaction in the presence of aluminium ion. *Colloids and Surfaces A: Physicochemical and Engineering Aspects* 168(1): 1–12.

Eslinger E and Peaver D (1988) *Clay Minerals for Petroleum Geologists and Engineers, SEPM Short Course n° 22. Soc*. Tulsa, OK: Economic Paleontologists and Mineralogists.

Feng X, Simpson AJ and Simpson MJ (2005) Chemical and mineralogical controls on humic acid sorption to clay mineral surfaces. *Organic Geochemistry* 36(11): 1553–1566.

Ghabbour EA, Davies G, O'Donaughy K, et al. (1998) Adsorption of a plant-and a soil-derived humic acid on the common clay kaolinite. *Special Publication-Royal Society OF CHEMISTRY* 228: 185–194.

Giles CH, Smith D and Huitson A (1974) A general treatment and classification of the solute adsorption isotherm. I. Theoretical. *Journal of Colloid and Interface Science* 47(3): 755–765.

Hamoud HI, Finqueneisel G and Azambre B (2017) Removal of binary dyes mixtures with opposite and similar charges by adsorption, coagulation/flocculation and catalytic oxidation in the presence of CeO_2/H_2O_2 Fenton-like system. *Journal of Environmental Management* 195: 195–207.

Holtzapffel T (1985) Clays minerals: Preparation, diffractometric analysis and determination. *Société géologique du Nord* 12: 1–136.

Jozja N (2003) *Study of Albanian clay materials. "Multi-scale" characterization of a magnesium bentonite*. PhD thesis, University of Orléans, Orléans, France.

Kpangni EB, Andji YYJ, Adouby K, et al. (2008) Mineralogy of clay raw materials from Cote d'ivoire: Case of the deposit from Katiola. *Journal of Applied Sciences* 8: 871–875.

Lin J and Zhan Y (2012) Adsorption of humic acid from aqueous solution onto unmodified and surfactant-modified chitosan/zeolite composites. *Chemical Engineering Journal* 200: 202–213.

Madejova J and Komadel P (2001) Baseline studies of the clay minerals society source clays: Infrared methods. *Clays and Clay Minerals* 49(5): 410–432.

Majzik A and Tombácz E (2007) Interaction between humic acid and montmorillonite in the presence of calcium ions I. Interfacial and aqueous phase equilibria: Adsorption and complexation. *Organic Geochemistry* 38(8): 1319–1329.

Peng X, Luan Z, Chen F, et al. (2005) Adsorption of humic acid onto pillared bentonite. *Desalination* 174(2): 135–143.

Rauthula MS and Srivastava VC (2011) Studies on adsorption/desorption of nitrobenzene and humic acid onto/from activated carbon. *Chemical Engineering Journal* 168(1): 35–43.

Rouquerol F, Rouquerol J and Sing K (1999) *Adsorption by Powders and Porous Solids: Principles, Methodology and Application*. London: Academic Press.

Salman M, El-Eswed B and Khalili F (2007) Adsorption of humic acid on bentonite. *Applied Clay Science* 38(1): 51–56.

Schwarzenbach RP, Gschwend PM and Imboden DM (2003) *Environmental Organic Chemistry*. New Jersey: John Wiley Sons.

Shen J, Gagliardi S, McCoustra MR, et al. (2016) Effect of humic substances aggregation on the determination of fluoride in water using an ion selective electrode. *Chemosphere* 159: 66–71.

Sing KS (1985) Reporting physisorption data for gas/solid systems with special reference to the determination of surface area and porosity (Recommendations 1984). *Pure and Applied Chemistry* 57(4): 603–619.

Tang Y, Liang S, Yu S, et al. (2012) Enhanced adsorption of humic acid on amine functionalized magnetic mesoporous composite microspheres. *Colloids and Surfaces A: Physicochemical and Engineering Aspects* 406: 61–67.

Terashima M, Fukushima M and Tanaka S (2004) Influence of pH on the surface activity of humic acid: micelle-like aggregate formation and interfacial adsorption. *Colloids and Surfaces A: Physicochemical and Engineering Aspects* 247: 77–83.

Tombácz E and Szekeres M (2006) Surface charge heterogeneity of kaolinite in aqueous suspension in comparison with montmorillonite. *Applied Clay Science* 34(1): 105–124.

Vieira AP, Santana SA, Bezerra CW, et al. (2009) Kinetics and thermodynamics of textile dye adsorption from aqueous solutions using babassu coconut mesocarp. *Journal of Hazardous Materials* 166(2): 1272–1278.

Vojkan M, Milan J, Snežana DJ, et al. (2017) The removal of lead (II) Ions from aqueous solutions by acid-activated clay modified with sodium carboxymethyl cellulose. *Applied Ecology and Environmental Research* 15(4): 1461–1472.

Wang J, Zhou Y, Li A, et al. (2010) Adsorption of humic acid by bi-functional resin JN-10 and the effect of alkali-earth metal ions on the adsorption. *Journal of Hazardous Materials* 176(1): 1018–1026.

Wang M, Liao L, Zhang X, et al. (2012) Adsorption of low concentration humic acid from water by palygorskite. *Applied Clay Science* 67: 164–168.

Wang S, Terdkiatburana T and Tadé MO (2008) Adsorption of Cu (II), Pb (II) and humic acid on natural zeolite tuff in single and binary systems. *Separation and Purification Technology* 62(1): 64–70.

Yan WL and Bai R (2005) Adsorption of lead and humic acid on chitosan hydrogel beads. *Water Research* 39(4): 688–698.

Zhang L, Luo L and Zhang S (2012) Integrated investigations on the adsorption mechanisms of fulvic and humic acids on three clay minerals. *Colloids and Surfaces A: Physicochemical and Engineering Aspects* 406: 84–90.

Zhou JL, Rowland S, Fauzi R, et al. (1994) The formation of humic coatings on mineral particles under simulated estuarine conditions—A mechanistic study. *Water Research* 28(3): 571–579.

Zhu X, He J, Su S, et al. (2016) Concept model of the formation process of humic acid–kaolin complexes deduced by trichloroethylene sorption experiments and various characterizations. *Chemosphere* 151: 116–123.